

Numerical simulation for a droplet fission process of electrowetting on dielectric device

Dongdong He^a, Huaxiong Huang^{b,*}, Yongji Tan^a

^a*Department of Mathematical Sciences, Fudan University, Shanghai, China*

^b*Department of Mathematics and Statistics, York University, Toronto, Canada*

Abstract

Electrowetting has been proposed as a technique for manipulating droplets surrounded by air or oil. In this paper, we discuss the modeling and simulation of the droplet fission process between two parallel plates inside an electrowetting on dielectric (EWOD) device. Since the gap between the plates is small, we use the two-phase Hele-Shaw flow as a model. An immersed boundary (IB) method is employed to solve the governing equations and a local level set method is used to track the drop interface. For comparison purposes, the same set of two-phase Hele-Shaw equations are also solved directly using the ghost-fluid (GF) method. Numerical results are consistent with experimental observations reported in the literature, provided that care is taken to treat the contact angle.

Key words: electrowetting, ghost fluid method, Hele-Shaw equations, immersed boundary method, local level set method, microfluidics, moving interface, two-phase flow.

1. Introduction

Lab-on-a-chip devices involve miniaturization of many chemical processes onto a single chip. Droplets, as the most common carrier for bio-chemical agents, have been found a growing importance in lab-on-a-chip design. Numerous papers which were centered on droplet operations have been published, c.f. [1]-[3] and references therein, and droplet-based lab-on-a-chip has been referred to as digital microfluidics. The basic operations include droplet generation; droplet translocation; droplet fusion and droplet fission.

* Corresponding Author

Email addresses: 061018014@fudan.edu.cn (Dongdong He), hhuang@yorku.ca (Huaxiong Huang), yjtan@fudan.edu.cn (Yongji Tan).

Amongst the different digital microfluidic systems, electrowetting on dielectric (EWOD) is one of the most promising technique to achieve these goals, because it manipulates discrete droplets rather than a continuous flow.

On the micro-scale, the surface tension forces play a dominate role in the hydrodynamics of a droplet. When a droplet contacts solid electrodes, a wetting force acts on the tri-phase contact line due to electrowetting (changes in the contact angle), and this can be utilized to manipulate the droplet. To avoid electrolysis, an insulating layer is usually inserted between the droplet and electrodes [4]-[6]. The applications of EWOD devices were discussed extensively in the literature, including microfluid transport [7], tunable optical fiber devices [8], rotating liquid micromotor [9], micro-injection [10], particle separation and concentration control [11]. Other studies focusing on the modeling of EWOD devices can be found in [3,5,12–15].

In this paper we investigate the droplet fission process using a two-phase Hele-Shaw model where the dynamics of both the droplet and the ambient flow is included. We present an immersed boundary (IB) method [16] as well as a ghost fluid (GF) method [17,18] to solve the Hele-Shaw equations. A local level set method [19] is used to track of the interface. Our numerical results show that the de-ionized water droplet pinches off without explicit tracking of the interface, contrarily to the method in [15] where value of the level set function needs to be artificially reduced to split the droplet.

The rest of the paper is organized as follows. Section 2 explains the basic principle of EWOD and provides a description of the parallel-plate EWOD device and relevant physical parameters. Section 3 presents the Hele-Shaw model for EWOD. Section 4 describes the numerical methods while numerical results are presented in Section 5. Discussion and conclusion are given in Section 6.

2. Basic principle of EWOD

It is well known that a droplet on a solid surface spreads or contracts until it has reached the state of minimum free energy, which is determined by cohesive forces in the liquid and the adhesion force between the liquid and the surface. At the tri-phase contact line, the relationship between contact angle θ and interfacial tensions is given by Young's equation

$$\cos \theta = \frac{\gamma_{SA} - \gamma_{SL}}{\gamma_{LA}} \quad (1)$$

where γ_{SA} is the solid-ambient fluid surface tension, γ_{SL} is solid-droplet liquid surface tension and γ_{LA} is the droplet liquid-ambient fluid interfacial tension.

When an electric voltage is applied, the change of electric charge distribution at the solid-liquid interface alters the free energy on the surface, inducing a change in wettability of the surface and the contact angle of the droplet [20], which is expressed by the Lippmann's equation [21]¹

$$\gamma_{SL}(V) = \gamma_{SL}(0) - \frac{c}{2}V^2 \quad (2)$$

¹ This equation is only valid under low and medium electric potentials. For higher voltages, experiments show that this relation is no longer valid. There exists a critical voltage beyond which the contact angle does not change any more. This is known as the contact angle saturation phenomena [22,23].

where c is the specific capacitance of the dielectric layer and V is the applied voltage. Combining (1) and (2) yields the Lippmann-Young equation

$$\cos(\theta_V) = \cos(\theta_0) - \frac{1}{2} \frac{cV^2}{\gamma_{LA}} \quad (3)$$

where θ_0 is the contact angle without voltage while θ_V is the contact angle with applied voltage V . This is known as electrowetting [22]. An insulating layer is usually inserted between the droplet and electrodes to avoid electrolysis.

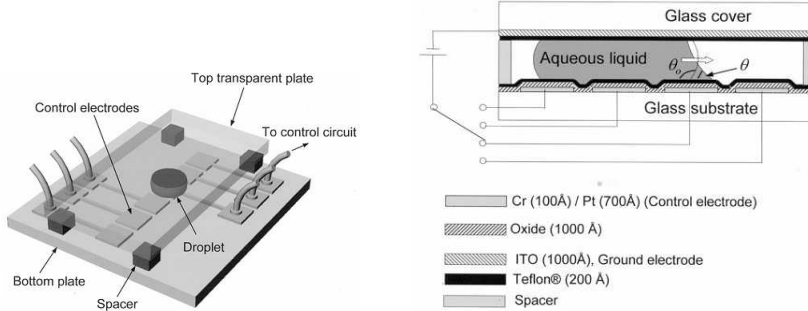


Fig. 1. Left: schematic of a parallel-plate EWOD device; right: cross-sectional view, reproduced from [3] (courtesy of C. J. Kim).

A schematic of an EWOD device is given in Figure 1. It consists of a glass cover, a top electrode (transparent plate) with hydrophobic Teflon coating ($\sim 200 \text{ \AA}$), spacers on each side of the droplet which assures the gap between the two plates is uniform ($\sim 70 \mu\text{m}$), a solid dielectric silicon dioxide ($\sim 1000 \text{ \AA}$) with Teflon coating ($\sim 200 \text{ \AA}$), control electrodes (bottom plate) and a glass substrate. Three different size of the control electrodes ($1.4 \text{ mm} \times 1.4 \text{ mm}$, $1.0 \text{ mm} \times 1.0 \text{ mm}$, $0.7 \text{ mm} \times 0.7 \text{ mm}$) are used in [3]. By adjusting the voltages of the electrodes, the droplets can be moved or split due to the change of wetting property of the two plates. This is the basic principle of the EWOD device.

3. Mathematical model

We assume that both droplet and ambient fluids are incompressible and their motion is governed by the incompressible Navier-Stokes equations

$$\nabla \cdot \mathbf{u} = 0 \quad (4)$$

$$\rho(\mathbf{u}_t + \mathbf{u} \cdot \nabla \mathbf{u}) = -\nabla p + \mu \Delta \mathbf{u} \quad (5)$$

in Ω_+^* and Ω_-^* , where $\mathbf{u} = (u, v, w)$ is the velocity, p is the pressure, ρ and μ are the density and dynamic viscosity, $\Omega^* = \Omega \times [0, H]$ is the whole domain, Ω_+^* and Ω_-^* are the regions of ambient fluid and droplet fluid respectively. Here Ω is the projection of Ω^* on to the parallel plates, and H is the gap width between two plates. On the droplet liquid-ambient liquid interface, the jump conditions must be satisfied [24]

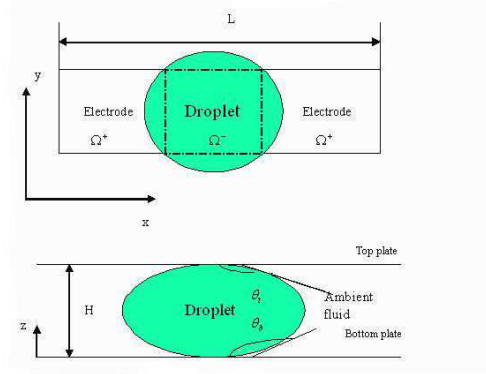


Fig. 2. EWOD device geometry. the above figure gives the top view while the bottom figure gives the side view of the EWOD device.

$$\begin{bmatrix} \left(\begin{array}{c} \mathbf{n} \\ \mathbf{t}_1 \\ \mathbf{t}_2 \end{array} \right) (pI - \tau)\mathbf{n} \end{bmatrix} = \begin{pmatrix} \sigma_{LA}\kappa \\ 0 \\ 0 \end{pmatrix} \quad (6)$$

where \mathbf{n} is unit normal vector, \mathbf{t}_1 and \mathbf{t}_2 are orthogonal unit tangent vectors, I is the identity matrix, κ is the local curvature of the interface, τ is the viscous stress tensor for incompressible flow, σ_{LA} is the interfacial tension between droplet fluid and ambient fluid, as stated earlier, and finally “[.]” denotes the jump across the interface.

3.1. Hele-Shaw equations

We non-dimensionalize the Navier-Stokes equation based on the following scalings

$$x^* = \frac{x}{L}, y^* = \frac{y}{L}, z^* = \frac{z}{H}, u^* = \frac{u}{U}, v^* = \frac{v}{U}, w^* = \frac{w}{V}, t^* = \frac{t}{L/U}, p^* = \frac{p}{\frac{\mu UL}{H^2}}. \quad (7)$$

Substituting (7) into the mass conservation (4), we obtain

$$\frac{\partial u^*}{\partial x^*} + \frac{\partial v^*}{\partial y^*} + \frac{VL}{UH} \frac{\partial w^*}{\partial z^*} = 0 \quad (8)$$

Thus $V = \frac{HU}{L} = \varepsilon U$ with $\varepsilon = \frac{H}{L}$. Non-dimensionalization for the momentum equations (5), yields

$$Re \cdot \varepsilon \left(\frac{\partial u^*}{\partial t^*} + u^* \frac{\partial u^*}{\partial x^*} + v^* \frac{\partial u^*}{\partial y^*} + w^* \frac{\partial u^*}{\partial z^*} \right) = -\frac{\partial p^*}{\partial x^*} + \varepsilon^2 \left(\frac{\partial^2 u^*}{\partial x^{*2}} + \frac{\partial^2 u^*}{\partial y^{*2}} \right) + \frac{\partial^2 u^*}{\partial z^{*2}} \quad (9)$$

$$Re \cdot \varepsilon \left(\frac{\partial v^*}{\partial t^*} + u^* \frac{\partial v^*}{\partial x^*} + v^* \frac{\partial v^*}{\partial y^*} + w^* \frac{\partial v^*}{\partial z^*} \right) = -\frac{\partial p^*}{\partial y^*} + \varepsilon^2 \left(\frac{\partial^2 v^*}{\partial x^{*2}} + \frac{\partial^2 v^*}{\partial y^{*2}} \right) + \frac{\partial^2 v^*}{\partial z^{*2}} \quad (10)$$

$$Re \cdot \varepsilon^3 \left(\frac{\partial w^*}{\partial t^*} + u^* \frac{\partial w^*}{\partial x^*} + v^* \frac{\partial w^*}{\partial y^*} + w^* \frac{\partial w^*}{\partial z^*} \right) = -\frac{\partial p^*}{\partial z^*} + \varepsilon^4 \left(\frac{\partial^2 w^*}{\partial x^{*2}} + \frac{\partial^2 w^*}{\partial y^{*2}} \right) + \varepsilon^2 \frac{\partial^2 w^*}{\partial z^{*2}} \quad (11)$$

where the Re is the Reynolds number defined by $Re = \frac{\rho UL}{\mu}$.

Since the gap width $H \sim 100\mu\text{m}$ is much smaller than the length $L \sim 1\text{mm}$, we have $\varepsilon \sim 0.1$. In addition, the Reynolds number $Re \sim 0.1$ is small. Dropping the high order term of ε and Re yields (in dimensional form)

$$\frac{\partial u}{\partial x} + \frac{\partial v}{\partial y} + \frac{\partial w}{\partial z} = 0, \quad (12)$$

$$\mu \frac{\partial^2 u}{\partial z^2} = \frac{\partial p}{\partial x}, \quad (13)$$

$$\mu \frac{\partial^2 v}{\partial z^2} = \frac{\partial p}{\partial y}, \quad (14)$$

$$\frac{\partial p}{\partial z} = 0. \quad (15)$$

We integrate the above equations in z and apply the no-slip condition² $\mathbf{u}|_{\partial\Omega^*} = 0$. Since (15) implies that p is independent of z , Integrating equation (12)-(15) respect to z yields the two-dimensional classical Hele-Shaw equations

$$u = -\frac{H^2}{12\mu} p_x, \quad (16)$$

$$v = -\frac{H^2}{12\mu} p_y, \quad (17)$$

$$0 = \frac{\partial u}{\partial x} + \frac{\partial v}{\partial y}, \quad (18)$$

which are valid both inside and outside the droplet. On the droplet and ambient fluid interface Γ , we apply the Young-Laplace relation

$$[p] = \sigma_{LA}\kappa, \quad (19)$$

where the mean curvature of the interface κ is approximated by

$$\kappa = \kappa_{xy} + \kappa_z. \quad (20)$$

Here κ_{xy} represents the curvature on the xy plane (parallel the plates) while κ_z represents the curvature of a cross-sectional of the interface along z direction, assuming that it is a circular arc as shown in Figure 2. After a simple calculation (see also [15]), we find that

$$\kappa_z = -\frac{\cos(\theta_t) + \cos(\theta_b)}{H} \quad (21)$$

where θ_t and θ_b are the contact angles on the top and bottom plates, respectively, c.f. Figure 2. For the device under consideration, we have $\theta_t = \theta_0$ and θ_b given by the Lippmann-Young equation (3). Our final condition at the interface is given by

$$[\mathbf{u}] = \left[-\frac{H^2}{12\mu} \nabla p \right] = 0 \quad (22)$$

where $\mathbf{u}=(u, v)$ is the two dimensional velocity vector.

² It is well-known that the no-slip condition leads to an non-integrable singularity in the pressure at the moving contact line. A popular remedy is to use a slip condition and we have also implemented the slip condition. However, our numerical tests show that there is almost no difference between the two formulations for the problem considered in this paper.

3.2. Immersed boundary formulation

We can re-cast the set of Hele-Shaw equations with the interface jump conditions into a single set of equations valid in the entire domain, including the interface, using the immersed boundary formulation

$$\mathbf{u} = -\frac{H^2}{12\mu} \left(\nabla p - \sigma_{LA} \int_{\Gamma} \kappa \delta(\mathbf{x} - \mathbf{x}_{\Gamma}) d\mathbf{x}_{\Gamma} \right), \quad (23)$$

$$0 = \nabla \cdot \mathbf{u}. \quad (24)$$

Here $\delta(\mathbf{x})$ is the Dirac-delta function. Using the signed distant ϕ as the level-set function for the interface, we can further simplify the immersed boundary formulation as

$$u = -\frac{H^2}{12\mu} (p_x - \sigma_{LA} \kappa \delta(\phi) n^1), \quad (25)$$

$$v = -\frac{H^2}{12\mu} (p_y - \sigma_{LA} \kappa \delta(\phi) n^2), \quad (26)$$

$$0 = \frac{\partial u}{\partial x} + \frac{\partial v}{\partial y} \quad (27)$$

where n^1 and n^2 are the projections of the normal vector \mathbf{n} on the x and y axes, respectively.

4. Numerical Methods

In this paper we use two numerical methods to solve the Hele-Shaw equations. In the first approach we use a level-set based IB method based on the immersed boundary formulation. We also implement the GF method by imposing the jump conditions directly for comparison purposes. All the discretizations are based on the nondimensional form of the Helw-Shaw equations using the following scalings

$$x^* = \frac{x}{L}, y^* = \frac{y}{L}, u^* = \frac{u}{U}, v^* = \frac{v}{U}, p^* = \frac{p}{\frac{\sigma_{LA}}{L}}. \quad (28)$$

The non-dimensional equations are, after dropping the superscript *,

$$\mathbf{u} = \beta \nabla p, \quad (29)$$

$$\nabla \cdot \mathbf{u} = 0 \quad (30)$$

for \mathbf{x} in Ω^+ and Ω^- with jump conditions

$$[p] = \kappa_{xy} + \frac{\kappa_z}{S}, \quad (31)$$

$$[\mathbf{u}] = [\beta \nabla p] = 0 \quad (32)$$

on Γ where

$$\beta = \begin{cases} \beta_+ \triangleq -\frac{S^2}{12\eta Ca}, & \mathbf{x} \in \Omega_+, \\ \beta_- \triangleq -\frac{S^2}{12Ca}, & \mathbf{x} \in \Omega_-. \end{cases} \quad (33)$$

Here $Ca = \frac{\mu_- U}{\sigma_{LA}}$ is the capillary number, $S = \frac{H}{L}$, $\eta = \frac{\mu_+}{\mu_-}$, κ_{xy} is the non-dimensional curvature in the xy plane and

$$\kappa_z = -\cos(\theta_t) - \cos(\theta_b). \quad (34)$$

In the following, we first describe the discretization, which is followed by a discussion of the local level-set method, the IB approach, and finally the GF method.

4.1. Discretization

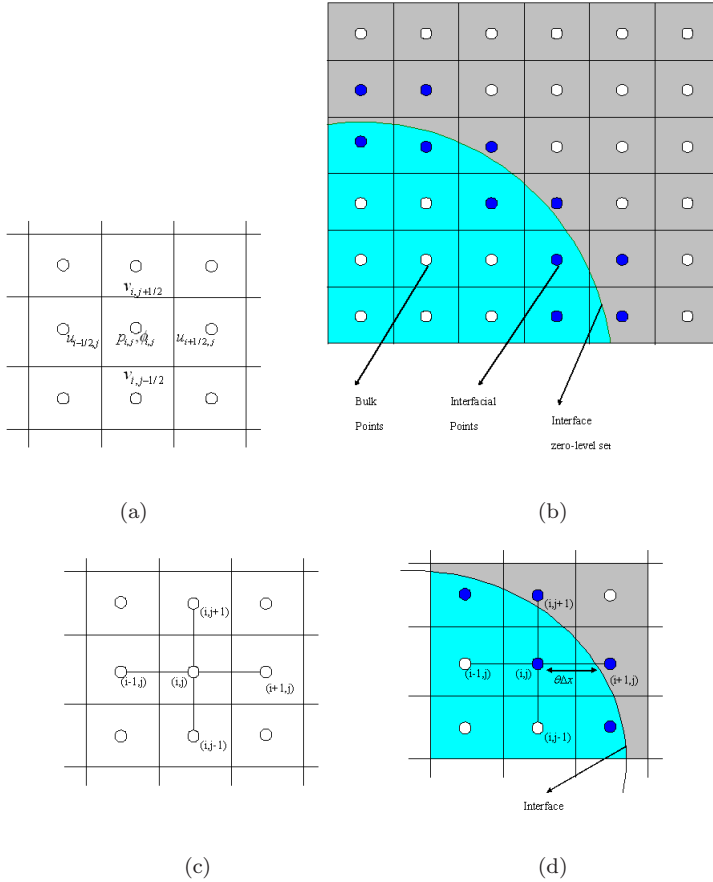


Fig. 3. (a) Schematics of the stagger grids; (b) Definitions of interior and interfacial points. The interface is given by the 0-level set. (c) Standard 5-point stencil for the interior points; (d) The configuration of a typical interfacial point (i, j) .

We use uniform spatial mesh size $\Delta x = \Delta y = h$ in the domain Ω and Δt is the time step. Set $N = 1/\Delta x = 1/\Delta y$ and use x_i to denote the i -th point in x direction, $i = 0, \dots, N$, and y_j and t_n are used in a similar manner. Following [25], we use a staggered grid shown in Figure 3, with the values of pressure p and level set function ϕ

stored at the center of each cell while the velocity components u and v stored on the face of the cells, c.f. Figure 3(a), as follows

$$\begin{aligned}\phi_{i,j}^n &= \phi(x_{i-1/2}, y_{j-1/2}, t_n), & p_{i,j}^n &= p(x_{i-1/2}, y_{j-1/2}, t_n), \\ u_{i-1/2,j} &= u(x_{i-1}, y_{j-1/2}), & u_{i+1/2,j} &= u(x_i, y_{j-1/2}), \\ v_{i,j-1/2} &= v(x_{i-1/2}, y_{j-1}), & v_{i,j+1/2} &= v(x_{i-1/2}, y_j).\end{aligned}$$

Here $x_{i-1/2} = x_i - h/2$ and $y_{j-1/2} = y_j - h/2$ for $i, j = 1, 2, \dots, N$.

4.2. Interface capturing using a local level set method

The level set technique is used to capture the moving interface in this paper. We define the a level set function ϕ which takes negative values inside and positive ones outside the droplet and the droplet interface corresponds to the zero level set. The evolution of ϕ is given by the transport equation [26]

$$\phi_t + u\phi_x + v\phi_y = 0. \quad (35)$$

The level set function is initially set to be a signed distance function on the whole computation domain Ω defined as

$$\phi(x, y, 0) = \begin{cases} d, & \text{if } (x, y) \in \Omega^+, \\ 0, & \text{if } (x, y) \in \Gamma(0), \\ -d, & \text{if } (x, y) \in \Omega^- \end{cases} \quad (36)$$

where $\Gamma(t) = \{(x, y) : \phi((x, y), t) = 0\}$ represents the droplet fluid-ambient fluid interface which is initially a circle on the xy plane.

Equation (35) is a first-order advection equation. We use a fifth-order upwind HJ WENO scheme [27] to discretize the spatial derivatives, and a third-order TVD Runge-Kutta scheme [28] for the time derivative of ϕ . After applying the evolution equation, the level set function is no longer a signed distance function, one normally needs to reinitialize ϕ , e.g., using a Hamilton-Jacobi equation

$$\begin{cases} \phi_t + s(\phi)H_G(\phi, \nabla\phi) = 0, \\ \phi(x, y, 0) = \phi_0(x, y), \end{cases} \quad (37)$$

with

$$H_G(\nabla\phi) = |\nabla\phi| - 1 \quad \text{and} \quad s(\phi) = \frac{\phi}{\sqrt{\phi^2 + |\nabla\phi|^2 \Delta x^2}}. \quad (38)$$

In the computation, $H_G(\nabla\phi)$ is approximated by the Godunov formula [19,27]

$$\begin{aligned}H_G(\phi_x^+, \phi_x^-, \phi_y^+, \phi_y^-) &= \\ &\begin{cases} \sqrt{(\max((\phi_x^+)^-, (\phi_x^-)^+))^2 + (\max((\phi_y^+)^-, (\phi_y^-)^+))^2} - 1, & \text{if } \phi_{i,j} \geq 0, \\ \sqrt{(\max((\phi_x^+)^+, (\phi_x^-)^-))^2 + (\max((\phi_y^+)^+, (\phi_y^-)^-))^2} - 1, & \text{otherwise.} \end{cases} \end{aligned} \quad (39)$$

Here $(a)^+ = \max(a, 0)$, $(a)^- = -\min(a, 0)$, ϕ_x^+ , ϕ_x^- , ϕ_y^+ and ϕ_y^- are spatial derivatives calculated using the HJ WENO scheme. The reinitialization process is achieved by solving the following equation to steady state

$$\phi_{i,j}^{n+1} = \phi_{i,j}^n - s(\phi_{i,j}^n) \hat{H}_G(\phi_{i,j}^n, \nabla \phi_{i,j}^n) \Delta t. \quad (40)$$

The above method is relatively expansive to implement since the reinitialization is done on the entire domain at each time step. In order to reduce the computation cost, we use a local level set method [19] in this paper. We define a cut-off function for the level set function ϕ as

$$c(\phi) = \begin{cases} 1, & \text{if } |\phi| \leq \gamma_1, \\ (|\phi| - \gamma_2)^2(2|\phi| + \gamma_2 - 3\gamma_1)/(\gamma_2 - \gamma_1)^2, & \text{if } \gamma_1 \leq |\phi| \leq \gamma_2, \\ 0, & \text{if } |\phi| \geq \gamma_2. \end{cases} \quad (41)$$

For a signed level set function $\phi^n(\mathbf{x})$ at the n -th time step, we define a tube T^n around the interface Γ^n with width γ_2 by

$$T^n = \{\mathbf{x} : |\phi^n(\mathbf{x})| < \gamma_2\}. \quad (42)$$

We update the level set function $\phi^n(\mathbf{x})$ inside the tube T^n by solving the following equation

$$\phi_t + c(\phi)u\phi_x + c(\phi)v\phi_y = 0 \quad (43)$$

for one time step, denoted by $\tilde{\phi}^{n+1}(\mathbf{x})$. The new location of the interface is given by $\Gamma^{n+1} = \{\mathbf{x} : \tilde{\phi}^{n+1}(\mathbf{x}) = 0\}$. Since $\tilde{\phi}^{n+1}(\mathbf{x})$ normally is not a signed distance function, we construct a signed distance function $\phi^{n+1}(\mathbf{x})$ as the new level set function in the neighborhood of Γ^{n+1} as follows. Let $d^{n+1}(\mathbf{x})$ be the distance function to the front Γ^{n+1} , denote

$$T^{n+1} = \{\mathbf{x} : |d^{n+1}(\mathbf{x})| < \gamma_2\}. \quad (44)$$

Here $d^{n+1}(\mathbf{x})$ is not yet known and our goal is to find a way to find its value so that a one-time-step updating can accomplished.

From the definition of the cut-off function (41), we know that the level set function is updated correctly in a tube of radius γ_1 . In the region $\{\mathbf{x} : \gamma_1 < |\phi^n| < \gamma_2\}$, the motion of level set function is modified by the cut-off function. Outside the tube T^n , the level set function is not updated. A steep gradient could develop at the region near the boundary of tube T^n . A reinitialization must be implemented in a region that contains T^{n+1} to reset $\tilde{\phi}^{n+1}$ be a signed distance function in a neighborhood of Γ^{n+1} of width γ_2 . Because of the CFL condition which requires $\Delta t \|\mathbf{u}\| < h$, the interface moves less than one grid point for a time step. We now can choose the region as

$$N^n = \{\mathbf{x} : |\phi^n(\mathbf{x} + \mathbf{y})| < \gamma_2, \text{ for } |\mathbf{y}| < h\}. \quad (45)$$

From the $\tilde{\phi}^{n+1}(\mathbf{x})$ above, we perform reinitialization in the tube N^n to obtain $d^{n+1}(\mathbf{x})$. Our new level set function is define as follows

$$\phi^{n+1}(\mathbf{x}) = \begin{cases} -\gamma_2, & \text{if } |d^{n+1}(\mathbf{x})| < -\gamma_2, \\ d^{n+1}(\mathbf{x}), & \text{if } |d^{n+1}(\mathbf{x})| \leq \gamma_2, \\ \gamma_2, & \text{if } |d^{n+1}(\mathbf{x})| > \gamma_2. \end{cases} \quad (46)$$

Note that this local level set method reinitializes in the tube around the interface periodically because a steep gradient may develop at the region near the boundary of the tube T [19]. The new level set function obtained from this procedure is not a signed distance function except inside the tube near the interface of width γ_2 . However, this is sufficient since the computation is only done inside the tube.

4.3. IB method

For numerical calculation based on the immersed boundary formulation, we first regularize the delta function by replacing $\delta(\phi)$ with

$$\delta_\varepsilon(\phi) = \begin{cases} 0, & \text{if } \phi < -\varepsilon, \\ \frac{1}{2\varepsilon} + \frac{1}{2\varepsilon} \cos\left(\frac{\pi\phi}{\varepsilon}\right), & \text{if } -\varepsilon \leq \phi \leq \varepsilon, \\ 0, & \text{if } \phi > \varepsilon. \end{cases} \quad (47)$$

We also use the regularized Heaviside function to approximate the viscosity

$$\mu = \mu_-((1 + (\eta - 1))H_\varepsilon(\phi)) \quad (48)$$

where

$$H_\varepsilon(\phi) = \begin{cases} 0, & \text{if } \phi < -\varepsilon, \\ \frac{1}{2} + \frac{\phi}{2\varepsilon} + \frac{1}{2\pi} \sin\left(\frac{\pi\phi}{\varepsilon}\right), & \text{if } -\varepsilon \leq \phi \leq \varepsilon, \\ 1, & \text{if } \phi > \varepsilon. \end{cases} \quad (49)$$

In numerical calculation, we use $\varepsilon = 1.5h$, following [29].

Using equations (28) and (25)-(27), we obtain the non-dimensional equations

$$\nabla \cdot \mathbf{u} = 0, \quad (50)$$

$$\mathbf{u} = \beta(\phi)(\nabla p - a(x, y)\delta_\varepsilon(\phi)\mathbf{n}) \quad (51)$$

with

$$\beta(\phi) = -\frac{S^2}{12(1 + (\eta - 1))H_\varepsilon(\phi)Ca}, \quad (52)$$

$$a(x, y) = \kappa_{xy} + \frac{\kappa_z}{S}, \quad (53)$$

$$\mathbf{n} = \frac{\nabla\phi}{|\nabla\phi|} \triangleq (n^1, n^2). \quad (54)$$

We discretize the equations as

$$u_{i+1/2,j} = \beta(\phi_{i+1/2,j}) \left(\frac{p_{i+1,j} - p_{i,j}}{h} - a_{i+1/2,j} \delta_\varepsilon(\phi_{i+1/2,j}) n_{i+1/2,j}^1 \right) \quad (55)$$

$$v_{i,j+1/2} = \beta(\phi_{i,j+1/2}) \left(\frac{p_{i,j+1} - p_{i,j}}{h} - a_{i,j+1/2} \delta_\varepsilon(\phi_{i,j+1/2}) n_{i,j+1/2}^2 \right) \quad (56)$$

where $\delta_\varepsilon(\phi_{i+1/2,j})$ is obtained by (47), $\beta(\phi_{i+1/2,j})$ by (49) and (52), and $n_{i+1/2,j}^1$ by (54). To compute $a_{i+1/2,j}$, we simply use interpolation from interpolation from $a_{i,j}$ and $a_{i+1,j}$,

which are the values of $a(\mathbf{x})$ at cell centers (i, j) and $(i + 1, j)$. More specifically, we use central finite difference method³ to compute κ_{xy} , which gives

$$\begin{aligned}\kappa_{xy} &= \nabla \cdot \frac{\nabla \phi}{|\nabla \phi|} \\ &= \frac{\phi_x^2 \phi_{yy} - 2\phi_x \phi_y \phi_{xy} + \phi_y^2 \phi_{xx}}{|\nabla \phi|^3} \\ &\approx \frac{(D_x^0 \phi_{i,j})^2 D_y^+ D_y^- \phi_{i,j} - 2D_x^0 \phi_{i,j} D_y^0 \phi_{i,j} D_y^0 D_x^0 \phi_{i,j} + (D_y^0 \phi_{i,j})^2 D_x^+ D_x^- \phi_{i,j}}{((D_x^0 \phi_{i,j})^2 + (D_y^0 \phi_{i,j})^2)^{1.5}}.\end{aligned}\quad (57)$$

To compute k_z , we tested two approaches. In both approaches use the contact angle obtained from the Lippmann-Young's equation (3) in the region of side electrodes. However, they differ in the region of middle electrode, where we assume that the contact angle remains unchanged in one approach while linear interpretation is used in the second one. Similarly, we can calculate $\delta_\varepsilon(\phi_{i,j+1/2})$, $\beta(\phi_{i,j+1/2})$, $n_{i,j+1/2}^2$, and $a_{i,j+1/2}$.

Substitute these equations into (61), we obtain the pressure equation on the entire domain

$$\begin{aligned}&\frac{\beta_{i-1/2,j}}{h^2} p_{i-1,j} + \frac{\beta_{i+1/2,j}}{h^2} p_{i+1,j} + \frac{\beta_{i,j-1/2}}{h^2} p_{i,j-1} + \frac{\beta_{i,j+1/2}}{h^2} p_{i,j+1} \\ &- \frac{\beta_{i-1/2,j} + \beta_{i+1/2,j} + \beta_{i,j-1/2} + \beta_{i,j+1/2}}{h^2} p_{i,j} = \\ &\frac{\beta_{i+1/2,j}}{h} a_{i+1/2,j} \delta_\varepsilon(\phi_{i+1/2,j}) n_{i+1/2,j}^1 - \frac{\beta_{i-1/2,j}}{h} a_{i-1/2,j} \delta_\varepsilon(\phi_{i-1/2,j}) n_{i-1/2,j}^1 \\ &+ \frac{\beta_{i,j+1/2}}{h} a_{i,j+1/2} \delta_\varepsilon(\phi_{i,j+1/2}) n_{i,j+1/2}^2 - \frac{\beta_{i,j-1/2}}{h} a_{i,j-1/2} \delta_\varepsilon(\phi_{i,j-1/2}) n_{i,j-1/2}^2\end{aligned}\quad (58)$$

where $\beta_{i+1/2,j}$ denotes $\beta(\phi_{i+1/2,j})$.

After the pressure is solved with proper boundary conditions, we can use

$$u_{i,j} = \frac{u_{i-1/2,j} + u_{i+1/2,j}}{2}\quad (59)$$

and

$$v_{i,j} = \frac{v_{i,j-1/2} + v_{i,j+1/2}}{2}\quad (60)$$

to find velocity (u, v) . These velocity in term will be used in the computation in (35) to update the level set function.

4.4. GF method

We start from the local mass conservation, ie, for each cell (i, j) the local conservation of mass gives

$$\frac{u_{i+1/2,j} - u_{i-1/2,j}}{\Delta x} + \frac{v_{i,j+1/2} - v_{i,j-1/2}}{\Delta y} = 0.\quad (61)$$

For interior points, we use the standard central difference to approximate the velocity at each cell face. If $\phi_{i,j} \leq 0$ and $\phi_{i+1,j} \leq 0$, we have

³ We should point out that we use one-sided finite difference to approximate κ_{xy} when the droplet is close to pinch off.

$$u_{i+1/2,j} = \frac{\beta^-(p_{i+1,j} - p_{i,j})}{\Delta x}. \quad (62)$$

And if both $\phi_{i,j} > 0$ and $\phi_{i+1,j} > 0$, then

$$u_{i+1/2,j} = \frac{\beta^+(p_{i+1,j} - p_{i,j})}{\Delta x}. \quad (63)$$

Velocity $u_{i-1/2,j}$, $v_{i,j+1/2}$ and $v_{i,j-1/2}$ are obtained similarly. Substituting these formulas into (61), we obtain the standard five-point difference equation for pressure on cell (i, j)

$$\frac{\beta^+}{\Delta x^2} p_{i-1,j} + \frac{\beta^+}{\Delta x^2} p_{i+1,j} + \frac{\beta^+}{\Delta y^2} p_{i,j-1} + \frac{\beta^+}{\Delta y^2} p_{i,j+1} - \left(\frac{2\beta^+}{\Delta x^2} + \frac{2\beta^+}{\Delta y^2} \right) p_{i,j} = 0 \quad (64)$$

for $\phi_{i,j} > 0$, and

$$\frac{\beta^-}{\Delta x^2} p_{i-1,j} + \frac{\beta^-}{\Delta x^2} p_{i+1,j} + \frac{\beta^-}{\Delta y^2} p_{i,j-1} + \frac{\beta^-}{\Delta y^2} p_{i,j+1} - \left(\frac{2\beta^-}{\Delta x^2} + \frac{2\beta^-}{\Delta y^2} \right) p_{i,j} = 0 \quad (65)$$

for $\phi_{i,j} \leq 0$.

For interfacial points, special attention is needed. The key of the GF method is to incorporate the pressure jump condition into the discrete Poisson equation for pressure. On a typical interfacial point (i, j) , cf. Figure3(d), denote the pressure at the interface and inside the droplet as p_Γ and

$$\alpha = \frac{|\phi_{i,j}|}{|\phi_{i,j}| + |\phi_{i+1,j}|}. \quad (66)$$

Since $\phi_{i,j} \leq 0$ and $\phi_{i+1,j} > 0$, the jump conditions at the interface (26) gives

$$\beta^- \frac{p_\Gamma - p_{i,j}}{\alpha \Delta x} = \beta^+ \frac{p_{i+1,j} - (p_\Gamma + [p]_\Gamma)}{(1 - \alpha) \Delta x}. \quad (67)$$

We obtain p_Γ from the above equation as

$$p_\Gamma = \frac{\beta^+ \alpha (p_{i+1,j} - [p]_\Gamma) + \beta^- (1 - \alpha) p_{i,j}}{\beta^+ \alpha + \beta^- (1 - \alpha)}. \quad (68)$$

From (29), we can use the following formula to compute the cell face velocity $u_{i+1/2,j}$.

$$u_{i+1/2,j} = \frac{\beta^- (p_\Gamma - p_{i,j})}{\alpha \Delta x} = \frac{\beta^+ \beta^-}{\beta^+ \alpha + \beta^- (1 - \alpha)} \frac{p_{i+1,j} - p_{i,j} - [p]_\Gamma}{\Delta x}. \quad (69)$$

The formula for velocity $u_{i-1/2,j}$, $v_{i,j+1/2}$ and $v_{i,j-1/2}$ are similar and the pressure equation at (i, j) can be obtained by substituting these velocity formulas into (61). To find pressure jump $[p]_\Gamma$, we note that

$$[p]_\Gamma = \kappa_{xy} + \frac{\kappa_z}{S} \triangleq a(\mathbf{x}_\Gamma) \quad (70)$$

and approximate $a(\mathbf{x}_\Gamma)$ by linear interpolation from the value $a_{i,j}$ and $a_{i+1,j}$.

Symbolically, we obtain the pressure Poisson equation for cell (i, j)

$$\frac{\beta_{i-1/2,j}}{h^2} p_{i-1,j} + \frac{\beta_{i+1/2,j}}{h^2} p_{i+1,j} + \frac{\beta_{i,j-1/2}}{h^2} p_{i,j-1} + \frac{\beta_{i,j+1/2}}{h^2} p_{i,j+1} - \frac{\beta_{i-1/2,j} + \beta_{i+1/2,j} + \beta_{i,j-1/2} + \beta_{i,j+1/2}}{h^2} p_{i,j} = F^x + F^y. \quad (71)$$

A more detailed discussion can be found in [18].

5. Numerical results

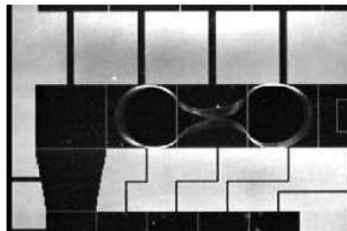


Fig. 4. Experimental observation of a splitting droplet in EWOD device (courtesy of C. J. Kim).

An experimental device for splitting a water droplet is shown in Figure 4. The voltages of three electrodes from left to right is 25, 0, and 25 V. This experiment was done in air environment, while other experiments [2] and [30] were carried out in the silicone-oil environment. In the above configuration, the threshold voltage to move the droplet is 12 V in silicone oil and 18 V in air [3]. The manipulation of droplets in air is much more challenging due to small contact angles and strong contact-angle hysteresis [3].

Table 1

Physical Parameters

Parameters	Values	Units
Channel Height H	70	μm
Electrode Length Scale $L_{electrode}$	1.4	mm
Computational Domain Length Scale L	$1.4 \times 3 = 4.2$	mm
Dynamic Viscosity Of Air μ^+	0.0000143	Pa·s
Dynamic Viscosity Of Water μ^-	0.00089	Pa·s
Interfacial Tension Of Water and Air γ_{LA}	71.99	mJ/m^2
Teflon Layer Height	200	\AA
Dielectric Constant Of Teflon	2	
Silicon Dioxide Layer Height	1000	\AA
Dielectric Constant Of Silicon Dioxide	3.8	
the droplet initial contact angle in silicone oil	117	$^\circ$
Applied Voltage	25	V

Our first set of computations is based on the device used in [3] in air environment. The physical parameters are listed in Table 1. In our computations, we use the 80×80 meshes. The numerical results using the ghost-fluid method are given in Figures 5 and 6 and those using the immersed boundary methods are given in Figures 7 and 8. It can be seen that our numerical results are sensitive to the contact angles used in the computation. For the method using the initial angle as the computational angle of middle electrode areas during the entire process, both results show that the droplet will not split automatically (see Figures 5 and 7). On the other hand, when linear interpolation is used to approximate

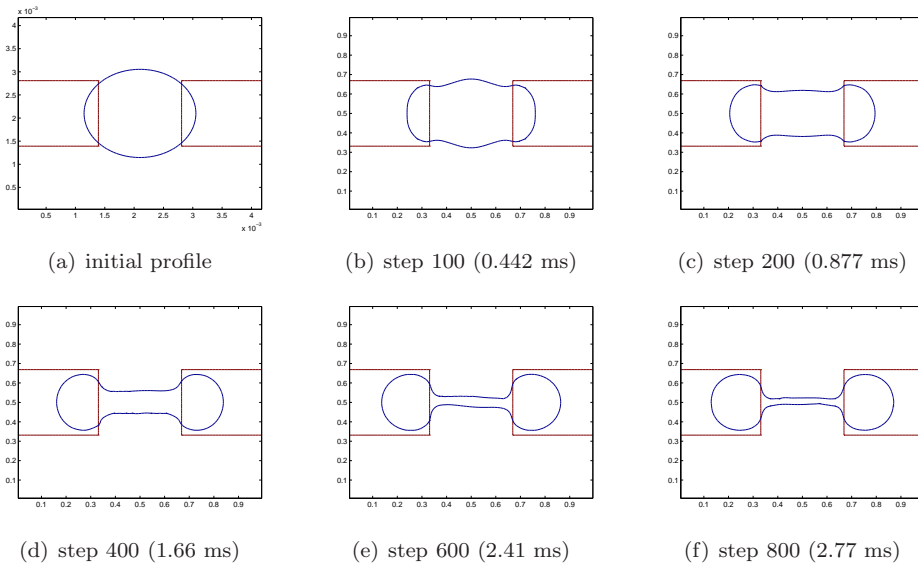


Fig. 5. Numerical simulation by the GF method using the initial contact angle.

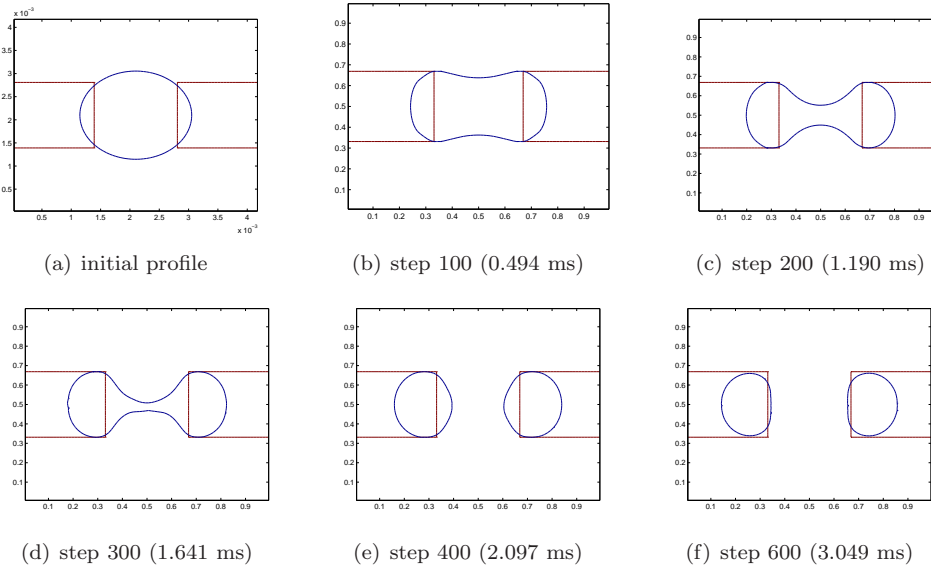


Fig. 6. Numerical simulation by the GF method using linear interpolation for the contact angle.

the contact angle, the results show that the droplet pinches off using both methods (see Figures 6 and 8), similar to experimental observations, c.f. Figure 4. However, there are some quantitative difference in the two results, the splitting time is not identical and the droplet shapes are not the same. Furthermore, the results of GF method shows that the droplet losses mass.

We now provide additional computations when parameter values are varied. For a

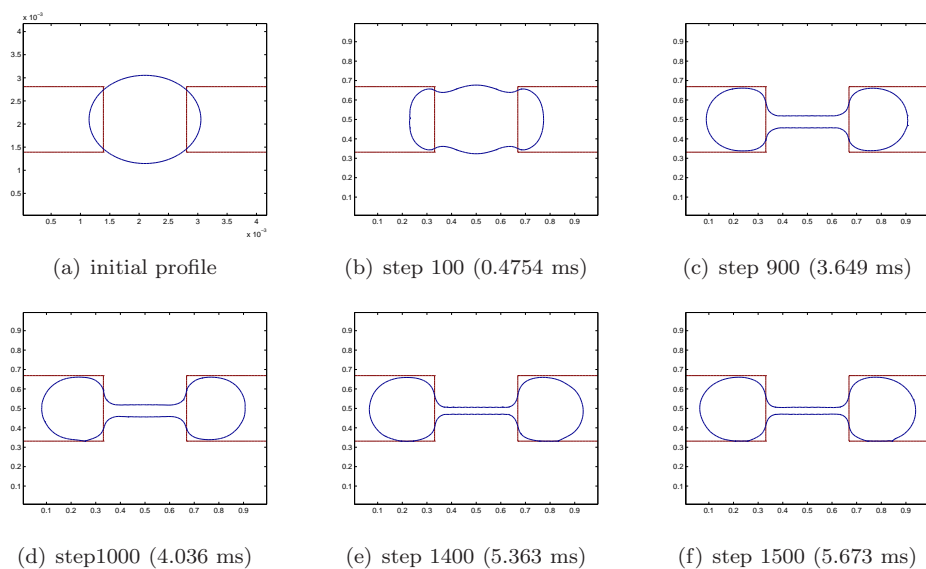


Fig. 7. Numerical simulation by the IB method using the initial contact angle.

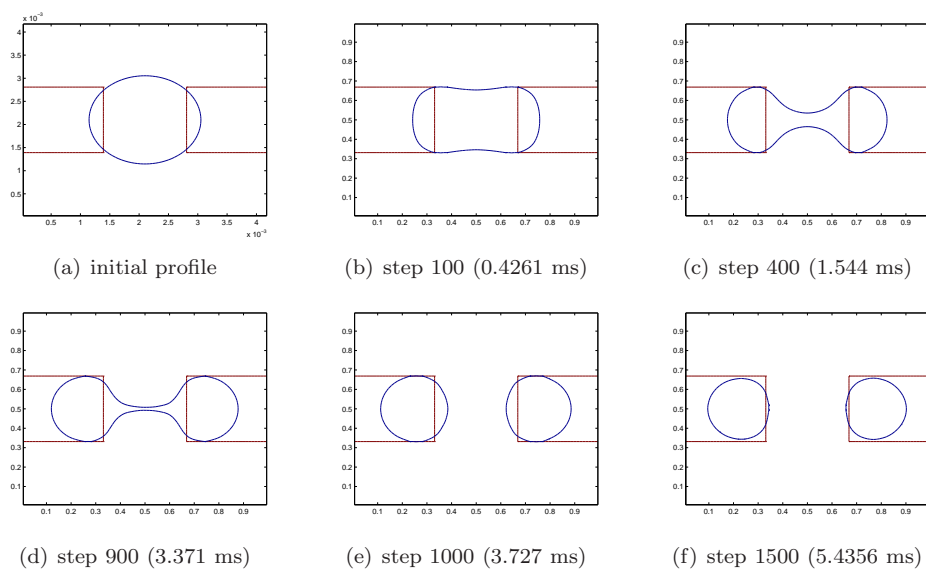


Fig. 8. Numerical simulation by the IB method using linear interpolation for the contact angle.

given device and a given environment (ambient flow), the droplet's initial contact angle is a fixed number as well as the ratio of height and length, and the applied voltage must be greater than a certain number so that the droplet can split. Here one of the most important parameters is the ratio of two viscosities η . In the following we present the simulations with two different η values, $\eta = 0.1$ and 10.

For $\eta = 0.1$, the results using GF and IB methods are shown in Figures 9 and 10,

Table 2
Computational Parameters

Parameters	Values	Units
Channel height scale H	70	μm
Electrode length scale $L_{electrode}$	1.4	mm
Applied Voltage	20	V
Computational domain length scale L	$1.4 \times 3 = 4.2$	mm
Interfacial tension of water and ambient flow scale γ_{LA}	33.1	mJ/m^2
Dynamic Viscosity Of Water μ^-	0.00089	$\text{Pa}\cdot\text{s}$
Water droplet initial contact angle in ambient flow θ_0	165	$^\circ$
Velocity scale U_0	0.001	m/s
Ratio of the device height and length $S = \frac{L}{L_{electrode}}$	0.0167	
Ratio of the viscosity of ambient flow and droplet η	I(0.1), II(10)	
Capillary Number $Ca = \frac{\mu^- U_0}{\gamma_{LA}}$	0.00003	

respectively. For $\eta = 10$, results for the two methods are shown in Figures 11 and 12. From these results, we can see that the droplet pinches off using both methods for both viscosities ratios. However, the time scale of these two methods are not identical. After further investigation (not shown here), we found that the droplet's splitting time is strongly correlated to the ratio of the viscosities. In our calculation, the droplet's splitting time for $\eta = 0.1$ is much less than that for $\eta = 10$.

6. Discussion and conclusions

This paper discusses EWOD modeling and simulation based on the two-dimensional two-phase Hele-Shaw equations. Both IB and GF methods, coupled with a local level-set method are used for the simulation.

As we point out earlier, the curvature κ_z plays a crucial role in the simulation. If we maintain the initial contact angle in the region of the middle electrode, the droplet does not pinch. On the other hand, if we allow the contact angle to vary, using linear interpolation, the results show that the droplet splits, in agreement with experimental observations. And our tests also show that the splitting of droplets slows down as the ratio of viscosities outside to inside the droplets increases. The simulations carried out in this paper do not include contact angle hysteresis and saturation effect, each plays an important role in the fission process. Nevertheless, our simulations produce a qualitative picture and useful insights into the understanding of the fission process.

Acknowledgements

The authors would like to thank Huisheng Zhang, Zheng Wu, Ian Mitchell, Hongkai Zhao and Wenbin Chen for helpful suggestions. The work was supported in part by Chinese NSF Project 10431030, NSERC and MITACS (Canada).

References

- [1] M.A. Burns, B.N. Johnson, S.N. Brahmaandra, K. Handique, J.R. Webster, M. Krishnan, T.S. Sammarco, P.M. Man, D. Jones, D. Heldsinger, C.H. Mastrangelo, and D.T. Burke, "An integrated nanoliter DNA analysis device." *Science*, 282: 484-487, 1998.
- [2] M.G. Pollack, A.D. Shenderov, and R.B. Fair, "Electrowetting-based actuation of droplets for integrated microfluidics." *Lab Chip*, 2: 96-101, 2002.
- [3] S.K. Cho, H. Moon and C.-J. Kim, "Creating, transporting, cutting, and merging liquid droplets by electrowetting-based actuation for digital microfluidic circuits." *J. Microelectromech. Syst.*, 12(1): 70-80, 2003.
- [4] J. Zeng and T. Korsmeyer, "Principles of droplet electrohydrodynamics for lab-on-a-chip." *Lab Chip*, 4: 265-277, 2004.
- [5] L.-S. Jang, G.-H. Lin, Y.-L. Lin, C.-Y. Hsu, W.-H. Kan, and C.-H. Chen, "Simulation and experimentation of a microfluidic device based on electrowetting on dielectric." *Biomed. Microdevices*, 9: 777-786, 2007.
- [6] L. Minnema, H. A. Barneveld, and P. D. Rinkel, "An investigation into the mechanism of water treeing in polyethylene high voltage cables." *IEEE Trans. Electr. Insul.*, EI-15: 461-472, 1980.
- [7] W. Satoh, M. Loughran, and F. Mugele, "Microfluidic transport based on direct electrowetting." *J. Appl. Phys.*, 96(1): 835-841, 2004.
- [8] F. Cattaneo, K. Baldwin, S. Yang, T. Krupenking, S. Ramchandran and J. A. Rogers, "Digitally tunable microfluidic optical fiber devices." *J. Microelectromech. Syst.* 12(6): 907-912, 2003.
- [9] J. Lee, C.-J. Kim, "Surface-tension-driven microactuation based on continuous electrowetting." *J. Microelectromech. Syst.*, 9(2): 171-180, 2000.
- [10] K. Hoshino, S.K. Fan, and C.-J. Kim, "Enhancement of mixing by droplet-based actuation for microinjection." *Proc. IEEE Conf. MEMS*, Maastricht, The Netherlands, 355-358, 2004.
- [11] S.K. Cho, and C.-J. Kim, "Particle separation and concentration control for digital microfluidic system." *Proc. IEEE 16th Annu. Int. Conf. MEMS*, Kyoto, Japan, 686-689, 2003.
- [12] B. Shapiro, H. Moon, R. Garrell, and C. J. Kim, "Equilibrium behavior of sessile drops under surface tension, applied external fields, and material variations." *J. Appl. Phys.*, vol.93, 2003.
- [13] J. Berthier, P. Clementz, O. Raccurt, D. Jary, P. Claustre, C. Peponnet and Y. Fouillet, "Computer aided design of an EWOD microdevice." *Sensors and Actuators*, 127: 283-294, 2006.
- [14] H.W. Lu, K. Glasner, A. L. Bertozzi, and C.-J. Kim, "A diffuse interface model for electric wetting droplets in a Hele-Shaw cell." *preprint*.
- [15] S.W. Walker and B. Shapiro, "Modeling the fluid dynamics of Electrowetting on Dielectric (EWOD)." *J. Microelectromech. Syst.*, 15(4): 986-1000, 2006.
- [16] M. Sussman, P. Smereka, and S. Osher, "A level set method approach for computing solutions to incompressible two-phase flow." *J. Comput. Phys.*, 114: 146-159, 1994.
- [17] M. Kang, R. Fedkiw, and X.-D. Liu, "A boundary condition capturing method for multiphase incompressible flow." *J. Sci. Comput.*, 15: 323-360, 2000.
- [18] X.-D. Liu, R.P. Fedkiw, and M. Kang, "A boundary condition capturing method for Poisson's Equation on irregular domains." *J. Comput. Phys.*, 160: 151-178, 2000.
- [19] D. Peng, B. Merriman, S. Osher, H. Zhao, and M. Kang, "A PDE-based fast local level set method." *J. Comput. Phys.*, 155: 410-438, 1999.
- [20] M. Vallet, B. Berge, and L. Vovelle, "Electrowetting of water and aqueous solutions on poly (Ethylene terephthalate) insulating films." *Polymer*, 37(12): 2465-2470, 1996.
- [21] M.G. Lippmann, "relations entre les phénomènes électriques et capillaires." *Ann. Chem. Phys.*, 5(11): 494-549, 1875.
- [22] H.J.J. Verheijen and M.W.J. Prins, "reversible electrowetting and trapping of charge: model and experiments." *Langmuir*, 15(20): 6616-6620, 1999.
- [23] M. Vallet, B. Berge, "Limiting phenomena for the spreading of water on polymer films by electrowetting." *Eur. Phys. J. B*, 11: 583-591, 1999.
- [24] L.D. Landau and E.M. Lifshitz, *Fluid Mechanics*. Pergamon Press, NY, 1978.
- [25] F. Harlow and J. Welch, "Numerical calculation of time-dependent viscous incompressible flow of fluid with free surface." *Phys Fluids* 8, 2182-2189, 1965.
- [26] S. Osher and J.A. Sethian, "Front propagating with curvature-dependent speed: algorithms based on Hamilton-Jacobi formulations." *J. Comput. Phys.*, 79(1): 12-49, 1988.

- [27] G. Jiang and D. Peng, "Weighted ENO schemes for Hamilton-Jacobi equations." *SIAM J. SCI. Comput.*, 21(6): 2126-2143, 2000.
- [28] C.W. Shu and S. Osher, "Efficient implementation of essentially non-oscillatory shock capturing schemes." *J. Comput. Phys.*, 77: 439-471, 1988.
- [29] S. Osher and R. Fedkiw, *Level Set Methods and Dynamic Implicit Surface*. Springer, NY, 2003.
- [30] J. Lee, H. Moon, J. Fowler, C.-J. Kim and T. Schoellhammer, "Addressable micro liquid handling by electric control of surface tension." *Proc. IEEE Int. Conf. MEMS, Interlaken, Switzerland*, 499-502, 2001.

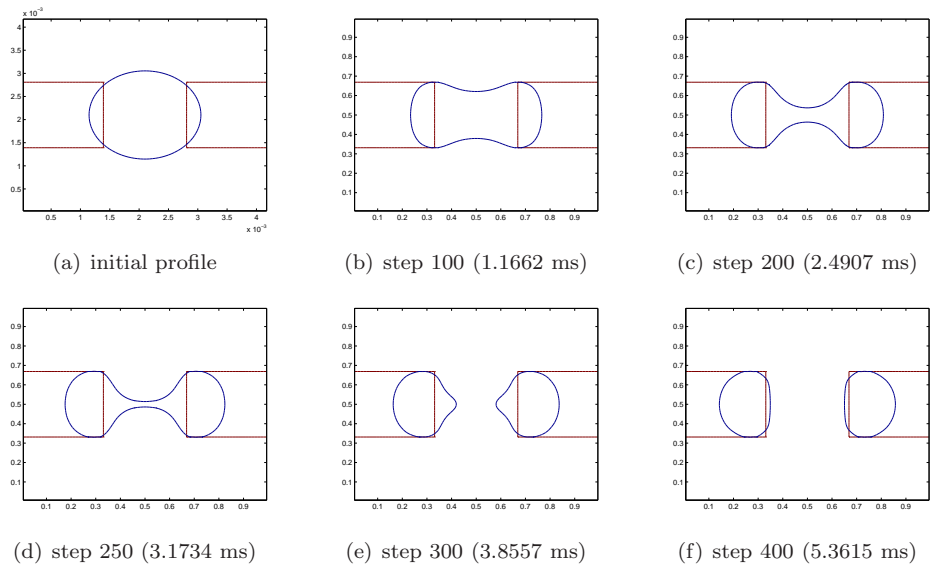


Fig. 9. Numerical simulation by the GF method for $\eta = 0.1$.

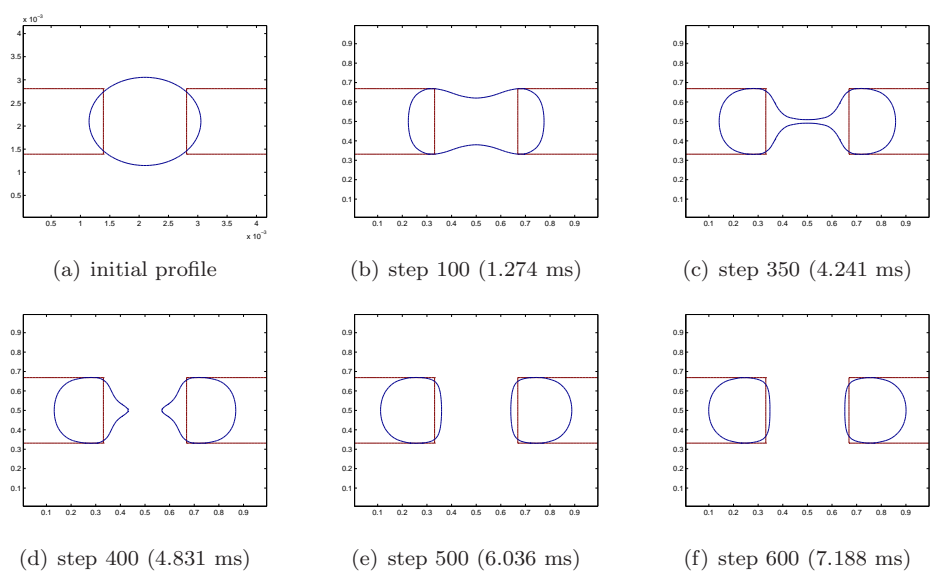


Fig. 10. Numerical simulation by the IB method for $\eta = 0.1$.

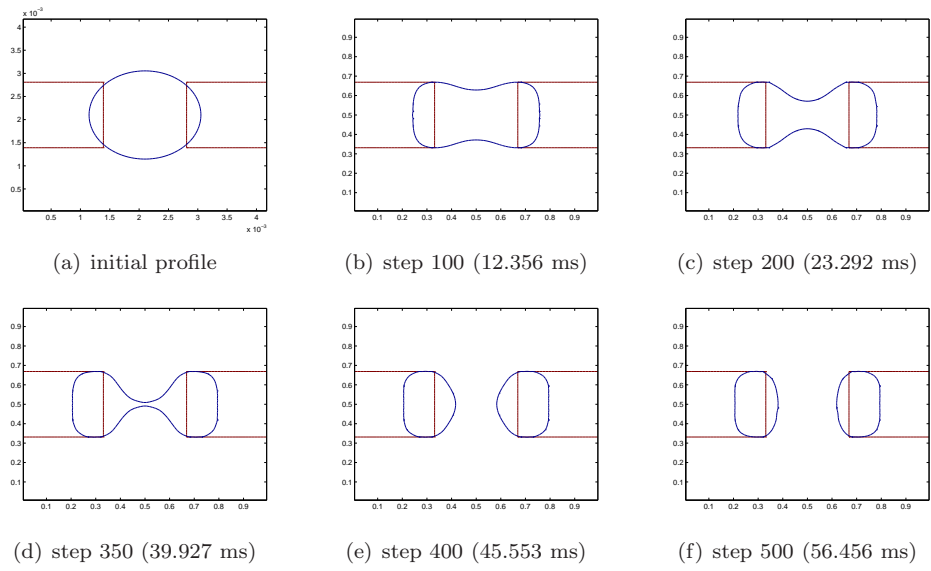


Fig. 11. Numerical simulation by the GF method for $\eta = 10$.

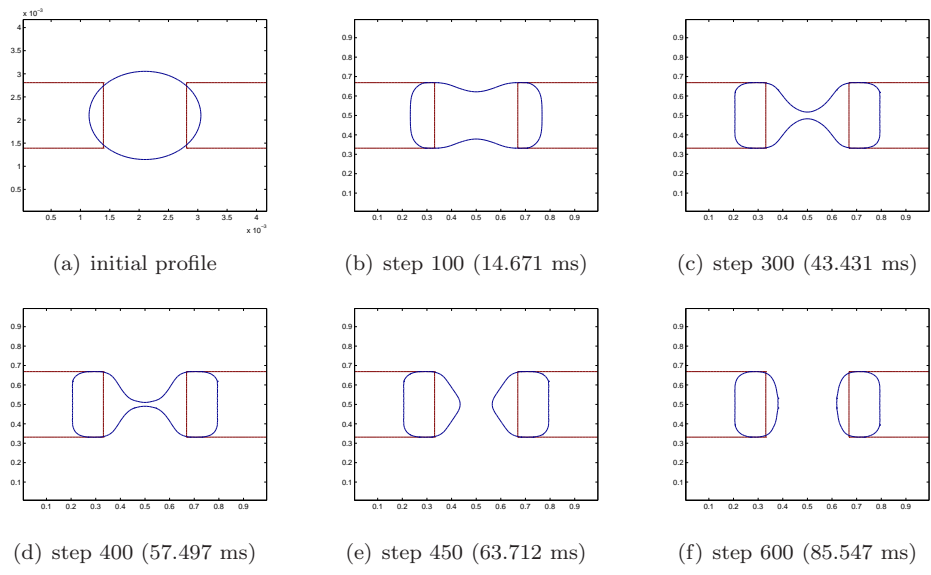


Fig. 12. Numerical simulation by the IB method for $\eta = 10$.